

Approximate and exact nodes of fermionic wavefunctions: coordinate transformations and topologies

Michal Bajlich, Lubos Mitas, Gabriel Drobny, and Lucas K. Wagner

Center for High Performance Simulation and Department of Physics,
North Carolina State University, Raleigh, NC 27695.

(Dated: March 22, 2024)

A study of fermion nodes for spin-polarized states of a few-electron ions and molecules with *s*; *p*; *d* one-particle orbitals is presented. We find exact nodes for some cases of two electron atomic and molecular states and also the first exact node for the three-electron atomic system in $^4S(p^3)$ state using appropriate coordinate maps and wavefunction symmetries. We analyze the cases of nodes for larger number of electrons in the Hartree-Fock approximation and for some cases we find transformations for projecting the high-dimensional node manifolds into 3D space. The node topologies and other properties are studied using these projections. We also propose a general coordinate transformation as an extension of Feynman-Cohen back flow coordinates to both simplify the nodal description and as a new variational freedom for quantum Monte Carlo trial wavefunctions.

PACS numbers: 02.70.Ss, 03.65.Ge

I. INTRODUCTION

The problem of fermion nodes is one of the most intriguing challenges in quantum simulations of fermionic systems by stochastic methods such as quantum Monte Carlo (QMC)^{1,2}. In QMC the many-fermion wavefunction is represented by an ensemble of sampling points (walkers) in the space of fermion coordinates. The walkers are propagated according to the matrix elements of the projector $\exp(-H)$ where H is a real parameter and H is a Hamiltonian. It is straightforward to show that the propagated wavefunction solves the time-dependent Schrödinger equation in imaginary time $\tau = it$ and converges to the ground state for $\tau \rightarrow \infty$. Unfortunately, for fermions such a straightforward sampling process runs into difficulties and the projection becomes very inefficient. The ensembles of walkers which initially sample negative and positive parts of the wavefunction are independent and asymptotically converge to the same (bosonic) distribution with an exponential growth of error bars for fermionic observables. In electronic structure QMC calculations³ this well-known fermion sign problem is circumvented by the fixed-node approximation which restricts the negative and positive walkers into separate regions of space defined by an approximate fermion node (zero boundary) of the best available trial/variational wavefunction. That guarantees stability of the statistical error bars at the price of a fixed-node bias. The fixed-node bias is proportional to the square of the nodal displacement error and therefore in typical electronic structure calculations the resulting bias is rather small. Even for hundreds of electrons, Hartree-Fock or multi-reference Hartree-Fock (HF) nodes lead to impressive accuracy when used within QMC. The fixed-node QMC calculations typically provide about 95% of the correlation energy in real systems³ such as molecules, clusters, solids, etc.

At a more fundamental level, knowledge of the exact node enables one to eliminate the fixed-node bias com-

pletely, and the exact energy can be calculated in time which scales as a low-order polynomial in the number of particles. Therefore elimination of the fixed-node error remains one of the intriguing possibilities for employing QMC to attack a number of important many-body problems which require accuracy beyond a few-determinant Hartree-Fock nodes.

Let us assume a system of spin-polarized electrons described by a real wavefunction $\Psi(R)$ where R denotes the electron spatial coordinates. The exchange of an electron pair with labels i, j , denoted as P_{ij} , gives $\Psi(R) = (P_{ij}\Psi)(R)$. Consequently, the antisymmetry implies that there exists a subset of electron configurations, called a fermion node, for which the wavefunction is zero. Let us eliminate the regions in which the wavefunction vanishes because of other reasons (eg, external potential); then the fermion node is given by an implicit equation

$\Psi(R) = 0$. In general, the fermion node is a $(ND-1)$ -dimensional manifold (hypersurface) assuming that we have N fermions in a D dimensional space. The fermion nodes of small systems, mostly atoms, were investigated in several previously published papers^{4,5,6,7,9}. The general properties of fermion nodes were analyzed in an extensive study by Ceperley¹⁰ which included a proof of the tiling property and generalizations of the fermion nodes to density matrices. We mention two of the results which will be used later.

i) Tiling property for the nondegenerate ground state: Let us define a nodal cell $\Omega(R_0)$ as a subset of configurations which can be reached from the point R_0 by a continuous path without crossing the node. The tiling property says that by applying all possible particle permutations to an arbitrary nodal cell of a ground state wavefunction one covers the complete configuration space. Note that this does not specify how many nodal cells are there. Furthermore, symmetry of the state is also symmetry of the node and tiling property is valid for any non-degenerate ground state within the given discrete symmetry.

ii) If two nodal surfaces cross each other they are or-

thogonal at the crossing. If n nodal surfaces cross each other, the crossing angles are all equal to π/n .

In addition, it was numerically shown¹⁰ that the nodal cells for a number of finite free particle systems are maximal, i.e., all regions with the same sign of wavefunction are interconnected. The fermion nodes for degenerate and excited states were further studied by Foulkes and co-workers¹¹. Recent interesting work by Bresanini, Reynolds and Ceperley revealed differences in the nodal surface topology between Hartree-Fock and correlated wavefunctions for the Be atom explaining the large impact of the $2s;2p$ near-degeneracy on the fixed-node QMC energy¹².

The remainder of this paper is organized as follows: in Sec. II we discover new exact fermion nodes for two and three-electron spin polarized systems. In Sec. III we categorize the nodal surfaces for the several half-filled subshells relevant for atomic and molecular states. In Sec. IV we suggest a general particle position transformation, both as a tool to simplify the description of the nodes and also as a possible new variational freedom for trial wavefunctions. Finally, in the last section we present our conclusions and suggestions for future work.

II. EXACT NODAL SURFACES

We assume the usual electron-ion Hamiltonian and we first investigate a few electron ions focusing on fermion nodes for subshells of one-particle states with $s; p; d; f; \dots$ symmetries using variable transformations, symmetry operations and explicit expressions for the nodes.

A. Three-electron quartet $^4S(p^3)$ state

Let us first analyze a special case with $r_1 = r_2$ and $r_{23} = r_{31}$. It is then easy to see that the inversion around the origin with subsequent rotations is equivalent to the exchange of two particles, say, 1 and 2 (Fig.1). Therefore for this particular configurations of particles the combination of parity and rotations is closely related to the exchange symmetry. The illustration also shows that the six distances do not specify the relative positions of the three electrons unambiguously. For a given set of the distances there are two distinct positions, say, of the electron 3, relative to the fixed positions of electrons 1 and 2 (see Fig.1) and compare positions 3 and 3" of the third electron.

In order to analyze the wavefunction in an unambiguous manner it is convenient to define new coordinates. Let us denote $\mathbf{r}_{12}^+ = \mathbf{r}_1 + \mathbf{r}_2; \mathbf{r}_{12}^- = \mathbf{r}_1 - \mathbf{r}_2$ together with the customary $\mathbf{r}_{12} = \mathbf{r}_1 - \mathbf{r}_2; \mathbf{r}_{12} = \mathbf{r}_1 - \mathbf{r}_2$. We can now introduce the following map of the Cartesian coordinates

$$(\mathbf{r}_1; \mathbf{r}_2; \mathbf{r}_3) \rightarrow (\mathbf{r}_{12}^+; \mathbf{r}_{12}^-; \mathbf{r}_3; \cos \theta; \cos \phi; \psi) \quad (1)$$

with definitions: $\cos \theta = \mathbf{r}_3 \cdot (\mathbf{r}_1 - \mathbf{r}_2) / (r_3 |\mathbf{r}_1 - \mathbf{r}_2|)$, $\cos \phi = \mathbf{r}_{12}^+ \cdot \mathbf{r}_{12}^- / (r_{12}^+ r_{12}^-)$ and ψ being an azimuthal an-

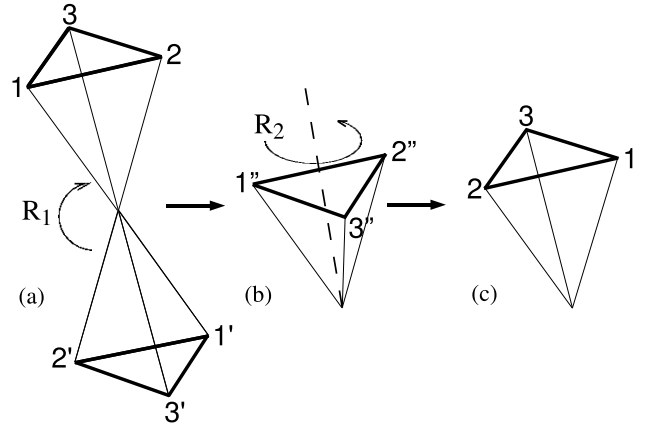


FIG. 1: Inversion and two subsequent rotations of three particles: (a) Original and inverted (primed) positions; (b) Positions after the rotation R_1 in the plane given by the particles 1, 2 and the origin; (c) Positions after the second rotation R_2 around the $\mathbf{r}_1 + \mathbf{r}_2$ axis. Note that the original positions of the particles 1 and 2 are exchanged.

gle of \mathbf{r}_3 in the relative coordinate system with unit vectors $\mathbf{e}_x = \mathbf{r}_{12}^+ / r_{12}^+, \mathbf{e}_z = \mathbf{r}_{12}^- / r_{12}^-, \mathbf{e}_y = \mathbf{e}_z \times \mathbf{e}_x$. For completeness, ψ denotes three Euler angles which fix the orientation of the three-particle system in the original coordinates (e.g., two spherical angles of $\mathbf{r}_1 - \mathbf{r}_2$ and an azimuthal angle of \mathbf{r}_{12}^+). Since the angles are irrelevant in S symmetry, the first six variables fully specify the relative positions of the three particles and the wavefunction dependence simplifies to $(\mathbf{r}_{12}^+; \mathbf{r}_{12}^-; \mathbf{r}_3; \cos \theta; \cos \phi; \psi)$. Consider now two symmetry operations which change the sign of the wavefunction and keep the distances unchanged: parity P_I and exchange P_{12} between particles 1 and 2. The exchange flips the sign of all three $\cos \theta; \cos \phi; \psi$ while the parity changes only the sign of $\cos \phi$. The action of $P_I P_{12}$ on leads to

$$(\psi; \cos \theta; \cos \phi; \psi) = (\psi; \cos \theta; \cos \phi; \psi) \quad (2)$$

showing that the wavefunction is even in the simultaneous sign flip $(\cos \theta; \cos \phi; \psi) \rightarrow (-\cos \theta; -\cos \phi; -\psi)$. Applying the exchange operator P_{12} to the wavefunction and taking advantage of the previous property gives us

$$(\psi; \cos \theta; \cos \phi; \psi) = (\psi; \cos \theta; \cos \phi; \psi) \quad (3)$$

suggesting that there is a node determined by the condition $\cos \theta = 0$. It is also clear that the same arguments can be repeated with exchanged particle labels 2 & 3 and 3 & 1 and we end up with the same nodal condition: $\mathbf{r}_3 \cdot (\mathbf{r}_1 - \mathbf{r}_2) = 0$. This shows that the node is encountered when all three electrons lie on a plane passing through the origin. Now we need to prove that this is the only node since there might possibly be other nodal surfaces not revealed by the parametrization above. The node given above clearly fulfills the tiling property and all symmetries of the state. Furthermore, the state is the lowest

quartet of S symmetry and odd parity (lower quartets such as $1s2s3s$, $1s2s2p$, and $1s2p^2$ have either different parity or symmetry) and for the ground state we expect that the number of nodal cells will be minimal. This is indeed true since the node above specifies only two nodal cells (one positive, one negative): an electron is either on one or the other side of the nodal plane passing through the remaining two electrons. Furthermore, any distortion of the node from the plane necessarily leads to additional nodal cells (see Fig. 2) which can only increase energy by imposing higher curvature (kinetic energy) on the wavefunction. This is basically the Feynman's argu-

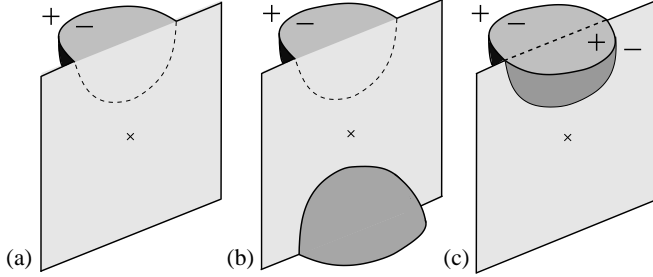


FIG. 2: (a) An illustration of an artificial distortion of the planar ground state node for the quartet state (see text); (b) The original and parity transformed distorted node; (c) Finally, a subsequent rotation of the inverted distortion necessarily leads to a new nodal pocket which is artificial for the ground state. In fact, nodes with similar topologies are present in excited states¹³.

ment from the proof demonstrating that the energy of fermionic ground state is always above the energy of the bosonic ground state (and also essentially the same argument as used for the proof of the tiling property¹⁰). In fact, as we show in another paper, higher excited states of this symmetry have additional nodes, as expected¹³. Given all the arguments above we conclude the proof that the plane is the exact node. Note that it is identical to the node of Hartree-Fock wavefunction of $2p$ orbitals given by $\Psi_{HF} = \det f(r)x; (r)y; (r)z$ where (r) is a radial function.

The coordinate transformation above is not the only one which can be used to analyze this state. The high symmetry of the problem enables us to find an alternative coordinate map with definitions of \cos modified to $\cos^0 = [(r_1 - r_2) \cdot r_{12}^+]/|r_1 - r_2| |r_{12}^+|$ and \cos^0 by redefinition of e_z to $e_z^0 = [(r_1 - r_2) \cdot r_{12}^+]/|r_1 - r_2| |r_{12}^+|$ and $e_y^0 = e_z \times e_x$. In the redefined coordinates the search for the node simplifies to an action of P_{12} on $(r_1^+, r_2; r_3; \cos; \cos^0; \cos^0)$

$$(\cos; \cos; \cos^0; \cos^0) = (\cos; \cos; \cos^0; \cos^0) \quad (4)$$

since the distances and $\cos^0; \cos^0$ are invariant to P_{12} . Obviously, this leads to the same nodal condition as derived above.

It is quite interesting to compare these two coordinate maps with $\cos; \cos^0$. Although parity and exchange

are independent operators the analysis above shows that in an appropriate coordinate system they imply the same nodal surface. Both these operators cause an identical sign change of the wavefunction indicating thus a special symmetry of the $^4S(p^3)$ ground state node which is higher than would be expected solely from antisymmetry. Similar observation was made in a study of fermion node in another case of two electron atomic state^{7,14}.

B. Two-electron triplet $^3P(p^2)$ and $^3g(p^2)$ states

Apparently, the exact node of this case was derived in a different context by Breit in 1930^{5,14}. Here we offer an independent proof which enables us to apply the analysis to some molecular states with the same symmetries. The exact node for the $^3P(p^2)$ state can be found in a similar way as in the case of quartet above. The state has even parity, cylindrical symmetry, say, around z -axis, and is odd under rotation by π around $x; y$ axes, $R(x), R(y)$. The mapping of Cartesian coordinates which enables to analyze the wavefunction symmetries is given by

$$(r_1; r_2) \rightarrow (r_1^+; r_2; \cos; \cos^0; \cos^0) \quad (5)$$

where $\cos = z_0 / |r_1 - r_2|$ with z_0 being the unit vector in the z -direction and \cos^0 being the azimuthal angle of $r_1 - r_2$; \cos^0 can be omitted due to the cylindrical symmetry. Further, \cos^0 is the azimuthal angle of r_1^+ in the relative coordinate system with the x -axis unit vector given by a projection of z_0 into the plane defined by $r_1; r_2$, i.e., $e_x = z_0 \times (r_1 - r_2)$, $e_z = (r_1 - r_2) \times (r_1 - r_2)$ and $e_y = e_z \times e_x$. Action of P_{12} on $R(x)$ reveals that the wavefunction is invariant in the simultaneous change $(\cos; \cos^0) \rightarrow (-\cos; \cos^0)$. This property and action of P_{12} to the wavefunction together lead to

$$(\cos; \cos; \cos^0; \cos^0) = (\cos; \cos; \cos^0; \cos^0) \quad (6)$$

with the rest of the variables unchanged. The node is therefore given by $\cos = 0$ and is encountered when an electron hits the plane which contains the z -axis and the other electron. As in the previous case the nodal plane fulfills the tiling property and manifestly divides the space into two nodal cells so that we can conclude that this node is exact. The exact node again agrees with the node of Hartree-Fock wavefunction $\Psi_{HF} = \det f(r)x; (r)y$.

The fixed-node QMC energies for the $^4S(p^3)$ and $^3P(p^2)$ cases derived above were calculated for a nitrogen cation with valence electrons in these states. The core electrons were eliminated by pseudopotentials²¹. The trial wavefunction was of the commonly used form with single HF determinant times a Jastrow correlation factor³. Note that the pseudopotential nonlocal s channel does not couple to either odd parity S state or even parity $P(p^2)$ state so that the nonlocal contribution to the energy vanishes exactly.

TABLE I: Total energies (a.u.) of N^+ , N^{++} and N^{+++} ions with core electrons eliminated by pseudopotentials. The energies are calculated by variational (VMC) and fixed-node diffusion (DMC) quantum Monte Carlo and Configuration Interaction (CI) methods. The HF energies are given as a reference for estimation of the correlation energies.

State	HF	CI	VMC	DMC
$^3P (p^2)$	-5.58528	-5.59491	-5.59491 (2)	-5.59496 (3)
$^4S (p^3)$	-7.24716	-7.27566	-7.27577 (1)	-7.27583 (2)
$^5S (sp^3)$	-8.98570	-9.02027	-9.01819 (4)	-9.01962 (5)

In order to compare the fixed-node QMC calculations with an independent method we have carried out also Configuration Interaction (CI) calculations with cc-pV6Z basis²² (with up to three g basis functions) which generates more than 100 virtual orbitals in total. In the CI method the wavefunction is expanded in excited determinants and we have included all single, double and triple excitations. Since the doubles and triples include two- and three-particle correlations exactly, the accuracy of the CI results is limited only by the size of the basis set. By comparison with other two- and three-electron CI calculations we estimate that the order of magnitude of the basis set CI bias is 0.01 mH (milliHartree) for two electrons and 0.1 mH and for three electrons (despite the large number of virtuals the CI expansion converges relatively slowly²⁰ in the maximum angular momentum of the basis functions, in our case $l_{max} = 4$). The pseudopotentials we used were identical in both QMC and CI calculations.

The first two rows of Tab. I show the total energies of variational and fixed-node DMC calculations with the trial wavefunctions with HF nodes together with results from the CI calculations. For $^3P (p^2)$ the energies agree within a few hundredths of mH with the CI energy being slightly higher but within two standard deviations from the fixed-node QMC result. For $^4S (p^3)$ the CI energy is clearly above the fixed-node DMC by about 0.17 mH as expected due to the limited basis set size. In order to illustrate the effect of the fixed-node approximation in the case when the HF node is not exact we have also included calculations for four electron state $^5S (sp^3)$ (for further discussion of this Hartree-Fock node see part III. below). For this case, we estimate that the CI energy is above the exact one by 0.3 mH so that the fixed-node energy is significantly higher than both CI and exact energies. Using these results we estimate that the fixed-node error is 1 mH, i.e., close to 3% of the correlation energy.

Since in the p^2 case we have assumed cylindrical symmetry, the derived node equation is applicable to any such potential, eg, equidistant homonuclear diatomic, trimers, etc, with one-particle orbitals $\chi_x; \chi_y$ which couple into the triplet state $^3g(x, y)$.

Note that the parametrization given above automati-

cally provides also one of the very few known exact nodes in atoms so far⁴, i.e., the lowest triplet state of He $^3S (1s2s)$. The spherical symmetry makes angles θ and ϕ irrelevant and simplifies the two-electron wavefunction dependence to distances $r_1; r_2; r_{12}$ or, alternatively, to $r_{12}; r_{12}^+; \cos \theta$. Applying P_{12} to wavefunction $(r_{12}; r_{12}^+; \cos \theta)$ leads to

$$(r_{12}; r_{12}^+; \cos \theta) = (r_{12}; r_{12}^+; -\cos \theta) \quad (7)$$

so that the node is given by the condition $\cos \theta = 0$, i.e., $r_1 = r_2 = 0$.

In addition, the presented analysis sheds some light on the He $^3P (1s2p)$ state node which was investigated before⁷ as having higher symmetry than implied by the wavefunction symmetries. The symmetry operations reveal that the wavefunction depends on $\cos \theta$ and that the node is related to the simultaneous flips such as $(\cos \theta; \phi) \rightarrow (-\cos \theta; \phi)$ or angle shifts $\phi \rightarrow \phi + \pi$. Since, however, two of the variables are involved, the node has a more complicated shape as the previous study illustrates⁷. In order to test the accuracy of the HF node we have carried out a fixed-node diffusion Monte Carlo calculation of the He $^3P (1s2p)$ state. The resulting total energy of -2.13320 (4) a.u. is in an excellent agreement with the estimated exact value of -2.13316⁸ which shows that the HF node is very close to the exact one¹⁵.

III. APPROXIMATE HARTREE-FOCK NODES

It is quite instructive to investigate the nodes of half-filled subshells of one-particle states with higher angular momentum.

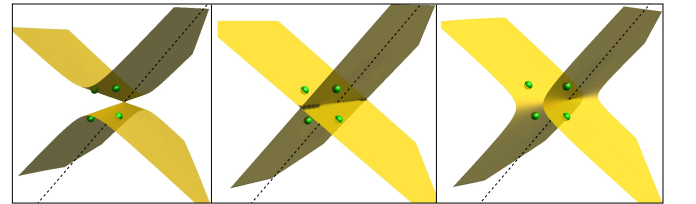


FIG. 3: (Color online) The 3D projected Hartree-Fock node of $^6S (d^5)$ state which is an elliptic cone (left and right pictures). The middle picture illustrates a case when two pairs of two electrons lie on orthogonal planes which pass through the origin. This two-plane node is of lower dimension because of the additional condition on positions of the electrons. It appears as a crossover between the cones with different orientation (left and right pictures). The small spheres show the positions of the four electrons while the line denotes the z axis.

A. Approximate Hartree-Fock node of ${}^6S(d^5)$ state

The HF determinant wavefunction for ${}^6S(d^5)$ is given

$$\Psi_{HF} = \frac{1}{\sqrt{5!}} (r_1) \det \begin{pmatrix} 2z^2 & x^2 & y^2 & x^2 & y^2 \\ xz & yz & xy & yz & xz \end{pmatrix} \quad (8)$$

where (r_1) is the radial part of the d-orbital and we assume that all the orbitals are from the same $l=2$ subshell, eg, 3d subshell. Since all radial functions are the same they factor out from the determinant and for the purpose of finding the node they can be omitted. The symmetry allows to rotate the system so that, say, electron 1 is on the z-axis, and then the corresponding column in the Slater matrix becomes $(2z_1^2; 0; 0; 0; 0)$. Assuming that $z_1 \neq 0$ we can then write the nodal condition as

$$\det \begin{pmatrix} x^2 & y^2 \\ xz & yz \end{pmatrix} = 0 \quad (9)$$

Using one of the electrons as a probe (ie, looking at the node from the perspective of one of electrons) we can find the projection of the node to 3D space. By denoting the probe electron coordinates simply as $(x; y; z)$ and by expanding the determinant we get

$$(x^2 - y^2)m_1 + xzm_2 + yzm_3 + xym_4 = 0 \quad (10)$$

where m_i are the corresponding cofactors. We divide out the first cofactor assuming that it is nonzero (not a crucial assumption as clarified below). We get

$$(x^2 - y^2) + axz + byz + cxy = 0 \quad (11)$$

where $a = m_2/m_1$, $b = m_3/m_1$, $c = m_4/m_1$. By completing the square this can be further rearranged to

$$(x - k_1 y)(x - k_2 y) + z(ax + by) = 0 \quad (12)$$

with $k_{1,2} = \frac{c}{c^2 + 4} = 2$. Let us define rotated and rescaled coordinates

$$u = (ak_2 - b)(x - k_1 y) = (k_1 - k_2) \quad (13)$$

$$v = (ak_1 - b)(x - k_2 y) = (k_1 - k_2) \quad (14)$$

$$w = z[(ak_1 - b)(ak_2 - b)] = (k_1 - k_2)^2 \quad (15)$$

so we can write the Eq. (11) as

$$uv + wu + wv = 0 \quad (16)$$

Note that this equation has a form which is identical to Eq. (10) with $m_1 = 0$ so this representation is correct for general m_1 . After some effort one finds that Eq. (16) is a cone equation (ie, d_{2^2} orbital) as can be easily verified by using the following identity

$$(2u^2 - v^2 - w^2) = 8 = uv + wu + wv \quad (17)$$

where $u = u + v + 2w$, $v = (u + v + 2w)$, $w = (u - v + 2w)$. The 3D projected node is therefore rotated and rescaled (elliptic) cone.

At this point it is useful to clarify how the derived node projection cone is related to the complete 14-dimensional node. Remarkably, the 3D projection enables us to understand some of the properties of the 14-dimensional manifold. First, the cone orientation and elliptic radii (ie, rescaling of the two axes with respect to the third one) are determined by the position of the four electrons in 3D space: with the exception of special lower dimensional cases explained below there always exists a unique cone given by the Eq. (16) which "fits" the positions of the four electrons. Besides the special cases (below) we can therefore define a projection of a single point in $4 - 3 = 12$ -dimensional space of four electrons onto a cone. That also implies that the complete 12-dimensional space describes a set (or family) of cones which are 3D projections of the nodal manifold. Similar projection strategies are often used in algebraic geometry to classify or analyze surfaces with complicated topologies and/or high dimensionalities.

Since the cone orientation and two radii are uniquely defined by the point in 12 dimensions and the cone itself is a 2D surface in 3D space of the probe electron the complete node then has $12 + 2 = 14$ dimensions. Therefore the d^5 HF node is a set of cone surfaces specified by the positions of the electrons. This particular form is simply a property of the d^5 Hartree-Fock determinant. From the derivation above it is clear that after factoring out the radial parts one obtains a homogeneous second-order polynomial in three variables with coefficients determined by the positions of the four electrons. In fact, from the theory of quadratic surfaces¹⁶, one finds that a general elliptic cone can possibly fit up to five 3D points/electrons, however, in our case the cone has an additional constraint. Our system was reoriented so that one of the electrons lies on the z-axis; that implies that the z-axis lies on the cone. Therefore the cone always cuts the xy (ie, $z = 0$) plane in two lines which are orthogonal to each other. The orthogonality can be verified by imposing $z = 0$ in Eq. (12) and checking that $k_1 k_2 = -1$. In addition, one can find "degenerate" configurations with two pairs of two electrons lying on orthogonal planes (Fig. 3). This corresponds to the "opening" of the cone with one of the elliptic radii becoming infinite and the resulting node having a form of two orthogonal planes (Fig. 3). Since in this case there is an additional condition on the particle positions, the two-plane node has lower dimension and is a zero measure subnode of the general 14-dimensional node. The condition is equivalent to $A_{44} = b^2 - a^2 - abc = 0$, where A_{44} is one of the quadratic invariants¹⁶. There are more special cases of lower dimensional nodes: a) when two electrons lie on a straight line going through the origin; b) when three electrons lie on a plane going through the origin; c) when four electrons lie in a single plane.

Remarkably, the analysis above enables us to find the

number of nodal cells. From Fig. 3 one can infer that by appropriate repositioning of the four electrons the cone surface smoothly "unwraps" the domains inside the cone, forms two crossing planes and then "wraps" around the cone domains of the opposite sign. That implies that an electron inside one of the cone regions can get to the region outside of the cone (with the same wavefunction sign) without any node crossing, using only appropriate concerted repositioning of the remaining four electrons. That enables us to understand that a point in the 15-dimensional space (positions of five electrons) can continuously scan the plus (or minus) domain of the wavefunction: there are only two maximal nodal cells.

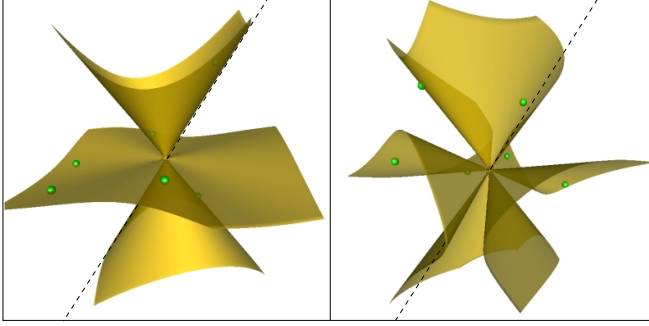


FIG. 4: (Color online) Projected Hartree-Fock node of $^8S(f^7)$ state. The node has two topologies: cone times planar surface or a cone "fused" with planar surface what form a single sheet surface. There is a smooth transition between these two forms depending on the positions of six electrons which are denoted by the small spheres. Note that the node contains the z axis which is denoted by the dashed line.

B. Approximate Hartree-Fock nodes of the $^8S(f^7)$ ion

We will use similar strategy as in the preceding case. After rotating one of the electrons to z -axis we expand the determinant in the probe electron column and eliminate the radial orbitals which form an overall prefactor of the Slater determinant since we assume that all seven f -states are from the same $l = 3$ subshell (eg, $4f$). We get

$$(m_1x + m_2y)(4z^2 - x^2 - y^2) + m_3z(x^2 - y^2) + m_4xyz + m_5x(x^2 - 3y^2) + m_6y(y^2 - 3x^2) = 0 \quad (18)$$

Note that the node contains the z -axis and there are two possible values of z for any x, y since the form is quadratic in z . This restricts the node shapes significantly and by further analysis one can find that the nodal surface projection into 3D has two topologies (Fig. 4). The first one is a cone times a planar surface (topologically equivalent to the Y_{40} spherical harmonic). Note that, in general, the planar surface is deformed from a straight plane since it

passes through the origin and, in addition, it is three of the electrons. The second topology is a "fused" cone and planar surface which results in a general single sheet cubic surface. The node transforms smoothly between these two topologies depending on how the six electrons move in space. These two topologies define the projection of the node into the probe 3D space and therefore enable us to capture the many-dimensional node for this particular Hartree-Fock state. This again enables to describe the complete node using a theorem from algebraic geometry which states that any cubic surface is determined by an appropriate mapping of six points in a projective plane^{17,18,19}. To use it we first need to realize the following property of the 3D projected node: The node equation above contains only a homogeneous polynomial in x, y, z which implies that in spherical coordinates the radius can be eliminated and the node is dependent only on angular variables. Hence, any line defined by an arbitrary point on the node and the origin (ie, a ray) lies on the node. In other words, we see that the surface is ruled, ie, it can be created by continuous sweep(s) of ray(s) passing through origin. This enables us to project the positions of the six electrons on an arbitrary plane which does not contain the origin and the node will cut such a plane in a cubic curve. As we mentioned above, a theorem from the algebraic geometry of cubic surfaces and curves says that any cubic surface is fully described by six points in a projective plane (see^{17,18,19}). For ruled surfaces any plane not passing through the origin is a projective plane and therefore we can specify a one to one correspondence between the $6 \times 3 = 18$ dimensional space and our cubic surface in 3D. Obviously, there will be a number of lower-dimensional nodes which will correspond to positions of electrons with additional constraints such as when they lie on curve with the degree lower than cubic; ie, a conic.

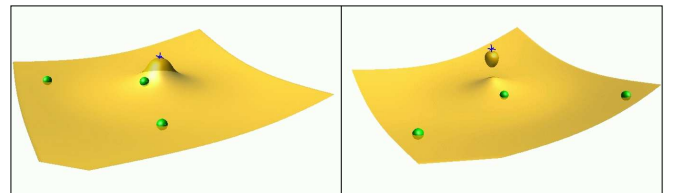


FIG. 5: (Color online) The 3D projection of the nitrogen cation $^5S(sp^3)$ Hartree-Fock node (the core electrons are eliminated by pseudopotentials). The projected node exhibits two topologies. It is either a planar surface deformed by the radial orbital functions at the nucleus or, in certain configurations, the deformation forms a small bubble detached from the surface (the picture on the right). The small cross is the location of the ion while the small spheres denote positions of electrons.

C . Approximate Hartree-Fock nodes of the ${}^5\text{S}(\text{sp}^3)$ ion

The HF node for this two-shell spin-polarized state can be investigated in a similar way as in previous cases with a new feature that the radial parts will be present in the expansion of the determinant. By expanding the determinant in the column of the probe electron with position $x; y; z$ the 3D node projection is simply given by

$$x + b^0y + c^0z + d^0(r) = 0 \quad (19)$$

where $b^0; c^0; d^0$ depend on ratios of cofactors and $(r) = \frac{s(r)}{p(r)}$ is the ratio of radial parts of s and p orbitals and $r = \sqrt{x^2 + y^2 + z^2}$. The probe electron will see a plane with a approximately bell-shape deformation in the area of the nucleus (See Fig. 5). The shape of deformation depends on the ratio of s and p radial parts and the magnitudes and signs of the cofactors. For certain configurations the deformation is so large that it gets detached from the surface and forms a separated ellipsoid-like bubble. The bubble results from the radial dependence of (r) which for pseudized core is not a monotonic function and therefore can create new topologies. Note that despite the fact that the 3D projection shows a separated region of space (the bubble) the complete node has again the minimal number of nodal cells property. To understand this, suppose that the probe electron is located inside the bubble and wavefunction there has a positive sign. Let us try to imagine how the electron can get to the other positive region (the other side of the planar surface). Seemingly, the electron would need to cross the nodal surface twice (the surface of the bubble and the planar surface). However, the complete node is a collective-coordinate object and by moving the other two electrons in an appropriate way the bubble attaches to the surface and then fuses into a single surface (Fig. 5, left) so that the probe electron can reach the positive region without node crossing.

In order to see whether the correlation would change the HF node we have carried out a limited study of the CI wavefunction nodes for this case; we have found some differences but we have not discovered any dramatic changes to the HF nodes. To quantify this further we have calculated the CI energy (with the same basis and level of correlation as in the previous cases) and the result is in the last row of Tab. I. We estimate that the fixed-node bias of the HF node is of the order of 0.001 Hartree which is close to 3% of the correlation energy. Obviously, the DMC energy is above the exact one and percentage-wise the amount of missing correlation energy is not insignificant. We conjecture that the HF node is reasonably close to the exact one although the details of the nodal surface are not captured perfectly.

D . Approximate Hartree-Fock nodes of spin-polarized p^3d^5 and sp^3d^5 shells with S symmetry

Let us for a moment assume a model wavefunction in which the radial parts of $s; p; d$ orbitals are identical. Then, using the arrangements similar to d^5 case, we can expand the determinant of p^3d^5 in one column and for the 3D node projection we then get

$$2u^2 - v^2 - w^2 + u + v + w = 0 \quad (20)$$

where $u; v; w$ are appropriate linear combinations of $x; y; z$. This can be further rewritten as

$$2(u + \frac{1}{4})^2 - (v - \frac{1}{2})^2 - (w - \frac{1}{2})^2 + \frac{1}{4} = 0 \quad (21)$$

where $\frac{1}{4} = (\frac{1}{2}^2 + \frac{1}{2}^2 + \frac{1}{2}^2) = \frac{3}{4}$. It is clear that the quadratic surface is offset from the origin (nucleus) by a vector normal to $u + v + w = 0$ plane. Using the properties of quadratic surfaces one finds that for $(\frac{1}{2}^2 + \frac{1}{2}^2 + \frac{1}{2}^2) < 2 = 3$, the node is a single-sheet hyperboloid with the radius $\frac{1}{2}$; otherwise it has a shape of a double-sheet hyperboloid. The double-sheet hyperboloid forms when there is an electron located close to the origin. A special case is a cone which corresponds to $(\frac{1}{4} = 0)$. The case of sp^3d^5 is similar, but with different $\frac{1}{4}$ which now has a contribution from the s -orbital (see Fig. 6). Once we include also the correct radial parts of orbitals in the $s; p; d$ channels the coefficients of the quadratic form depend on both cofactors and orbital radial functions. The resulting nodal surface is deformed beyond an ideal quadric and shows some more complicated structure around the nucleus (see Fig. 7) as illustrated on HF nodes of the majority spin electrons in Mn^{++} ion (note that the Ne-core electrons were eliminated by pseudopotentials).

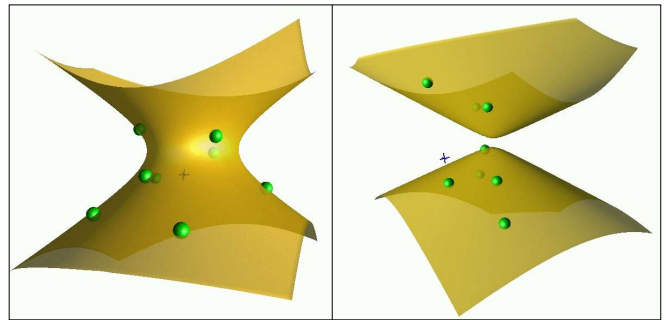


FIG. 6: (Color online) The 3D projection of the angular part of the ${}^{10}\text{S}(\text{sp}^3d^5)$ state Hartree-Fock node (with radial parts of orbitals identical for all sp^3d^5 orbitals). The projection has a topology of a single-sheet or double-sheet hyperboloid. The small cross shows the location of the nucleus while the spheres illustrate the electron positions.

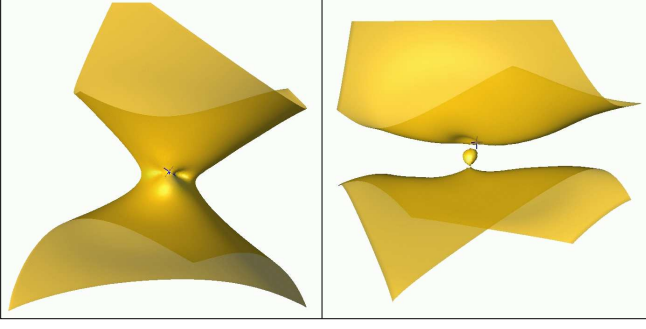


FIG. 7: (Color online) Projected Hartree-Fock node of $^{10}\text{S}(\text{sp}^3\text{d}^5)$ of the majority spin valence electrons in Mn^{+2} ion. The Ne-core electrons are eliminated by pseudopotentials. Note the deformations from the radial parts of orbitals, including a small bubble detached from the rest of the surface (the right picture). For clarity, the positions of electrons have been omitted.

IV. GENERALIZED ELECTRON COORDINATES

What we have learned from the previous cases is that for small number of electrons the Hartree-Fock wavefunctions display nodes which, if transformed in an appropriate way, lead to rather simple geometries.

In addition, it is instructive to consider how the nodal surfaces evolve with increasing number of electrons. Obviously, HF theory leads to low kinetic energies and the resulting mean-field nodes are very smooth. The exact nodes of the high symmetry $\text{P}(\text{p}^2)$ and $\text{S}(\text{p}^3)$ cases can be interpreted as reoriented planes which enable us to rotate one or two electrons and obviously such rotations do not cause any increase in the kinetic energy. For more particles the rotations and translations are not sufficient to rotate the electron positions and the lowest increase in kinetic energy in atomic systems is apparently produced by rescaling of the axes.

Finally, for larger number of electrons the node becomes more deformed and complex with possibilities of new topologies and topological changes. The 3D node projections we have analyzed above show that often there exist coordinate transformations which can simplify the node description and enable us to find useful node parametrizations (at least, for our cases of spin-polarized electronic subshells in ions). As we demonstrated on the $^3\text{P}(\text{p}^2)$ state similar spin-polarized open shells can be studied by analogous techniques as well.

In the analysis of the nodes we have presented a number of coordinate transformations and maps which enabled us to understand particular nodal structures and their topologies. It is interesting to explore this idea further and think about possible research directions. In order to illustrate some of the possibilities let us define a single-electron coordinate $\mathbf{r}_i \rightarrow \mathbf{r}_i'$ transformation as

$$\mathbf{r}_i' = \mathbf{M}_i(\mathbf{R})\mathbf{r}_i + \mathbf{t}_i(\mathbf{R}) \quad (22)$$

where $\mathbf{M}_i(\mathbf{R})$ is a metric tensor, $\mathbf{t}_i(\mathbf{R})$ is a spatial offset (translation) while \mathbf{R} represents coordinates of all electrons. The dependence of $\mathbf{M}_i(\mathbf{R})$ and $\mathbf{t}_i(\mathbf{R})$ on \mathbf{R} can be nonlinear and even include an explicit dependence on external potential to describe charge inhomogeneities or required symmetries. The antisymmetry condition further restricts the dependences of $\mathbf{M}_i(\mathbf{R})$ and $\mathbf{t}_i(\mathbf{R})$ on \mathbf{R} . Obviously the metric tensor has to be positive definite but otherwise the transformation is variationally free. Actually, the usefulness of this transformation can be twofold. First, as we mentioned, it can be employed as an efficient way to project the high-dimensional nodal manifold into a simpler, low-dimensional projection. Second, it can be useful as a new variational freedom to optimize the wavefunction nodes using the following form of a single determinant or linear combination of determinants

$$= \sum_k d_k \det_k f^{(k)}(\mathbf{r}_i') g \quad (23)$$

where $f^{(k)}g$ are one-particle orbitals and d_k are expansion coefficients. Therefore, besides optimizing the orbitals, one can also optimize the metric tensor and offset in order to get better variational wavefunctions and fixed-node energies. In fact, the transformation above can be considered a generalization of the Feynman-Cohen backflow quasiparticle coordinates²³. By simplifying $\mathbf{M}_i(\mathbf{R})$ to the unit matrix times a scalar function we can easily recover the backflow wavefunction which Feynman and Cohen suggested for liquid helium²³ and which was successfully employed in QMC in several previous studies^{24,25,26}. The new feature proposed here is the metric tensor which enables to better describe the systems with inhomogeneities and/or with rotation symmetries.

V. CONCLUSIONS

We have investigated the nodes of atomic and molecular spin-polarized systems with one-particle states in $s; p; d$ channels. We have studied cases with high symmetries which enabled us to find exact nodes for several states with a few electrons ($\text{p}^2; \text{p}^3; ^2$). Moreover, the projection of multi-dimensional manifolds into 3D space enabled us to study and characterize properties of nodes, in particular, their topologies for the Hartree-Fock wavefunctions. This analysis has provided useful insights and enabled us to formulate a general transformation of one-particle coordinates using coordinate translation (backflow) and metric tensor to capture inhomogeneities and/or rotation symmetries. Such transformations can be useful for understanding the nodal properties and topologies and also as a new variational freedom for QMC trial wavefunctions.

Acknowledgments

The support by ONR-N00014-01-1-0408, and NSF DMR-0121361, DMR-0121361 grants is gratefully ac-

knowledged. L.M. would like to thank D. Bressanini and P. Reynolds for discussions and N. Salwen for help in the early stages of this work.

-
- ¹ D.M. Ceperley and M.H. Kalos, in *Monte Carlo Methods in Statistical Physics*, edited by K. Binder, pp.145-194, Springer, Berlin, 1979; K.E. Schmidt and D.M. Ceperley, in *Monte Carlo Methods in Statistical Physics II*, pp.279-355, edited by K. Binder, Springer, Berlin, 1984.
 - ² B.L. Hammond, W.A. Lester, Jr., and P.J. Reynolds, *Monte Carlo Methods in ab initio quantum chemistry*, World Scientific, Singapore, 1994.
 - ³ M.W.C. Foulkes, L.M.itas, R.J. Needs and G. Rajagopal, *Rev. Mod. Phys.* 73, pp. 33-83 (2001).
 - ⁴ E.A. Hylleraas, *Z. Phys.* 54, 347 (1929); 48, 469 (1928).
 - ⁵ G. Breit, *Phys. Rev* 35, 569 (1930); D. Bressanini, private communication.
 - ⁶ J.B. Anderson, *J. Chem. Phys.* 63, 1499 (1975); 65 4121 (1976).
 - ⁷ J.B. Anderson, *Phys. Rev. A*, 35, 3550 (1987).
 - ⁸ C. Schwartz, *Phys. Rev. A* 134, 1181 (1964).
 - ⁹ W.A. Glauser, W.R. Brown, W.A. Lester, D. Bressanini, B.L. Hammond and M.L. Koszykowski, *J. Chem. Phys.* 97, 9200 (1992).
 - ¹⁰ D.M. Ceperley, *J. Stat. Phys.* 63, 1237, (1991).
 - ¹¹ W.M.C. Foulkes, R.Q. Hood and R.J. Needs, *Phys. Rev. B* 60, 4558 (1999).
 - ¹² D. Bressanini, D.M. Ceperley and P. Reynolds, in *Recent Advances in Quantum Monte Carlo Methods II*, Ed. W.A. Lester, S.M. Rothstein, and S. Tanaka, World Scientific, Singapore (2002).
 - ¹³ L.M. itas, G. Drobný, M. Bajlich, L.K. Wagner, in *Condensed Matter Theories*, Vol. 20, Eds. J.W. Clark and R. Pano, Nova Science Publishers, to appear.
 - ¹⁴ D. Bressanini and P.J. Reynolds, Unexpected symmetry in the nodal structure of the He atom, submitted.
 - ¹⁵ Another system with such symmetries is the H_2^+ (1s 2p) state, first analyzed by H.M. James, A.S. Coolidge, and R.D. Present, *J. Chem. Phys.* 4, 184 (1936).
 - ¹⁶ K. Rektorys, *Survey of Applicable Mathematics*, Kluwer, 1994.
 - ¹⁷ D. Pedoe, *Geometry Comprehensive Course*, Dover, New York, 1988.
 - ¹⁸ J.G. Semple, G.T. Kneebone, *Algebraic Projective Geometry*, Oxford University Press, Oxford, 1979.
 - ¹⁹ P. Griffiths and J. Harris, *Principles of Algebraic Geometry*, Wiley, New York, 1978.
 - ²⁰ W. Kutzelnigg, in *Explicitly Correlated Wave Functions in Chemistry and Physics*, Ed. J. Rychlewski, Kluwer, Dordrecht 2003, pp.4-82 and references therein.
 - ²¹ I. Ovcharenko, A. Aspuru-Guzik, W.A. Lester Jr., *J. Chem. Phys.* 114, 7790 (2001).
 - ²² A.K. Wilson, T.v. Mourik and T.H. Dunning, Jr., *J. Mol. Struct. (THEOCHEM)* 388, 339 (1997).
 - ²³ R.P. Feynman and M. Cohen, *Phys. Rev.* 102, 1189 (1956).
 - ²⁴ Y. Kwon, D.M. Ceperley and R.M. Martin, *Phys. Rev. B* 48, 12037 (1993); *ibid.* 50, 1684 (1994); *ibid.* 53, 7376 (1996); *ibid.* 58, 6800 (1998).
 - ²⁵ M. Holzmann, D.M. Ceperley, C. Pierleoni, and K. Esler *Phys. Rev. E* 68, 046707 (2003).
 - ²⁶ R.M. Pano and J. Carlson, *Phys. Rev. Lett.* 62, 1130 (1989).